JOURNAL OF Materials CHEMISTRY

Self-propagating high temperature synthesis of yttrium iron chromium garnets $Y_3Fe_{5-x}Cr_xO_{12}$ ($0 \leqslant x \leqslant 0.6$)

Maxim V. Kuznetsov,[a] Quentin A. Pankhurst,[a] Ivan P. Parkin,[b] Louise Affleck[b] and Yuri G. Morozov[c]

[a]*Department of Physics and Astronomy, University College London, Gower Street, London, UK WC1E 6BT. E-mail: q.pankhurst@ucl.ac.uk*
[b]*Department of Chemistry, University College London, 20 Gordon Street, London, UK WC1H 0AJ*
[c]*Institute of Structural Macrokinetics, Chernogolovka, Moscow Region, Russia 142432*

Received 15th November 1999, Accepted 22nd December 1999

Pure and chromium substituted yttrium iron garnets $Y_3Fe_{5-x}Cr_xO_{12}$ ($x = 0$, 0.1, 0.2, 0.3, 0.4, 0.5 and 0.6) have been made in air using self-propagating high-temperature synthesis (SHS), a combustion process involving the reaction of yttrium(III) oxide, iron(III) oxide, chromium(III) oxide, iron metal powder and sodium perchlorate. Two series of samples were produced: Series 1; SHS followed by annealing at 1450 °C for 4 h and series 2; SHS in a magnetic field of 1.1 T followed by annealing at 1450 °C for 4 h. SEM, EDAX, electron microprobe and IR measurements were carried out on both series of samples. X-Ray data showed that in all cases nearly single-phase garnets were produced. Room temperature Mössbauer data showed that the Cr exclusively substituted for Fe on the octahedral site sublattice. Magnetic hysteresis data showed that the series 2 samples had consistently larger magnetisations and smaller coercivities than the corresponding series 1 samples. This was attributed to microstructural effects, including a tendency to form larger sized crystallites in the presence of an applied field. The magnetic data also indicated a maximum in magnetisation and minimum in coercivity for both series 1 and series 2 samples with a Cr content of $x = 0.3$, the origins of which are discussed.

Introduction

Yttrium iron garnets ($Y_3Fe_5O_{12}$) have provoked great interest since their discovery by Bertaut and Forrat[1] and, independently, by Geller and Gilleo,[2] owing to their optical absorption and Faraday rotation effects (visible domain patterns).[3] Yttrium iron garnet is a very effective microwave filter and is exceptionally efficient as both a transmitter and transducer of acoustic energy. It crystallises in the garnet structure with a body centred cubic lattice (space group *Id*3*d*, no. 230), in which the yttrium atoms occupy position 24c, the oxygen atoms position 96h and the iron atoms position 24d (tetrahedral) and 16a (octahedral).

The magnetic properties of ferrite-garnets of general formula $M_3Fe_5O_{12}$ (M = lanthanide and yttrium) were first investigated by Pauthenet who established that these compounds (excluding M = Y, Sm, Eu, Lu) have compensation points for sublattice magnetic moments.[4,5] The Néel model for garnets involves three-sublattice components to explain the magnetic behaviour.[6] In this model ferrite-garnets are ferrimagnets, with three sublattices; *a*, *d* and *c*.[7–9] The large M^{3+} ions occupy the *c* sublattice which has eight-fold co-ordination sites. The iron atoms are found in two sites: the *a* sublattice, which is octahedral, and the *d* sublattice, which is tetrahedral. A magnetic moment of 5 μ_B per formula unit results from the negative super-exchange (antiferromagnetic) interaction between Fe^{3+} ions in the octahedral and tetrahedral sites through the intervening O^{2-} ions; it corresponds to the moment of one Fe^{3+} ion present in a tetrahedral site in excess of the number of Fe^{3+} ions in octahedral sites.[10] Ferrite-garnets have very complicated physical properties owing to interactions both within and between the sublattices. These materials have been investigated by substitutional doping to intensify or suppress the effects of the *a*, *d* or *c* sublattices. One such method is to substitute iron by magnetic or nonmagnetic ions on the tetrahedral and octahedral sites.

Yttrium iron garnets have some attractive features which make them amenable for study as model magnetic systems. The materials adopt cubic symmetry, have a definite composition, and contain only trivalent metal ions in the structure. Isovalent substitution of Fe^{3+} by magnetic or nonmagnetic M^{3+} ions can, in principal, change the resultant magnetic moments on both the octahedral or tetrahedral sublattice sites. The Curie temperature of yttrium iron garnet is lowered on isovalent substitution as the number of interactions of magnetic ions per formula unit is reduced.[11] One of the most widely used elements for isovalent substitution for the magnetic Fe^{3+} ion is Cr^{3+}.[10,12–18]

Standard methods for the preparation of pure and substituted yttrium iron garnet involves two steps, the processing of oxide mixtures or dried co-precipitated hydroxides, followed by heating. The initial step involves heating mixtures to 700–850 °C for 24 h. The second calcination step involves milling and pressing into pellets, followed by heating at 1350–1450 °C in oxygen or air for up to 16 h.[12,13]

Self-propagating high-temperature synthesis (SHS) is an alternative synthesis technique that involves a solid flame or synthesis wave. The reaction is driven by an exothermic chemical reaction.[19] This reaction is exothermic enough that when initiated at a point source it spreads through the whole reaction mixture.[20] The process is characterised by rapid synthesis involving extremely fast heating (*ca.* 1200 °C in 2–3 s) and cooling. In the ferrite-garnets system we have used SHS instead of the initial 24 h heating process. A notable aspect of SHS reactions is that the products often have high surface areas, high defect concentrations and are rapidly sintered. In this case such effects have enabled us to reduce the second firing stage to 4 h.

Here, we present the first preparation of pure and chromium-

substituted yttrium iron garnet by SHS. We also investigate the effect of an external magnetic field during the SHS combustion process and investigate the structural, magnetic and Mössbauer parameters of the products.

Experimental

All reagents were obtained from Aldrich Chemical Company (UK) and used as supplied. Manipulations, weighings and grindings were performed under a nitrogen atmosphere in a Saffron Scientific glove box. Self-propagating high-temperature synthesis reactions were carried out in air on pre-ground powders on a ceramic tile using sodium perchlorate as an internal oxygen source. Initial reaction compositions are given in Table 1. A heated nichrome filament (*ca.* 800 °C) was used to initiate the reactions. After SHS the products were washed with distilled water to remove co-produced NaCl. Sintering was carried out in a Carbolite rapid heating furnace with heating and cooling rates of 20 °C min^{-1}. Samples were ground after the SHS reaction and also after sintering; all measurements were recorded on powder samples. For the applied field SHS reactions a permanent Halbach cylinder magnet made by Magnetic Solutions Limited was used. This cylinder, comprising eight NdFeB magnets, provided a field of 1.1 T transverse to the cylinder axis. A quartz tube (22 mm outer diameter, 20 cm long) containing the green mixture was placed inside the Halbach cylinder prior to initiation of the combustion process.

X-Ray diffraction was performed in reflection mode on a Philips X-pert diffractometer using unfiltered Cu-Kα radiation ($\lambda_1 = 1.5405$ Å, $\lambda_2 = 1.5443$ Å). Vibrating sample magnetometry was carried out on an Aerosonic 3001 magnetometer in applied fields up to 7.5 kOe. ^{57}Fe Mössbauer spectra were recorded using a Wissel MR-260 constant acceleration spectrometer with a triangular drive waveform. The spectra were folded to remove baseline curvature and were calibrated relative to α-iron at room temperature. FTIR spectra were obtained as KBr pellets on a Nicholet 205 instrument. SEM/EDAX measurements were obtained using a Hitachi S570 instrument. Electron probe measurements were made on a JEOL EMA. The electron probe and EDAX measurements were standardised to Cr metal, Fe metal, quartz (for oxygen) and $Y_3Al_5O_{12}$ for yttrium.

Preparation of $Y_3Fe_{5-x}Cr_xO_{12}$ ($0 \leqslant x \leqslant 0.6$)

The same general reaction scale and procedure was used for all reactions, illustrated here for $Y_3Fe_{4.8}Cr_{0.2}O_{12}$.

Yttrium oxide (1.129 g, 5.0 mmol), iron(III) oxide (0.345 g, 2.16 mmol), chromium(III) oxide (0.0506 g, 0.33 mmol), iron metal (0.651 g, 11.6 mmol) and sodium perchlorate (0.535 g, 4.275 mmol) were ground together in a pestle and mortar. For the zero field reactions the green mixture was placed on a ceramic tile (*ca.* 1 cm by 7 cm strip) in air and a reaction initiated by a heated filament at one end. This produced a propagation velocity of *ca.* 2–3 mm s^{-1}. For the applied field reactions the green mixture was placed in a 22 mm od quartz tube and inserted into a 1.1 T Halbach cylinder permanent magnet. Some structuring of the green mixture was noted in the magnetic field, with the powder adopting an hour-glass shape in cross-section, centralised along the field lines, in the middle of the cylinder magnet.[21] This structuring persisted into the reaction products. The SHS reactions in the applied field were noted to have faster moving propagation waves of *ca.* 5 mm s^{-1} than those conducted in zero field. In all cases the resultant black powder was washed with distilled water (2×1 litres), filtered through a Buchner funnel and air dried. The powder was reground and heated to 1450 °C for 4 h. Yields in all reactions were essentially quantitative. The resultant powder was analysed by X-ray powder diffraction, Mössbauer spectroscopy, vibrating sample magnetometry, FTIR and SEM/EDAX.

CAUTION: SHS reactions can be explosively exothermic. All new reactions should be conducted on a small scale behind a safety screen. Also, sodium perchlorate is a powerful oxidising agent and can react violently with some metal powders. To alleviate this risk the Fe, Fe_2O_3, Cr_2O_3 and Y_2O_3 were ground in a pestle and mortar before the addition of $NaClO_4$. This mixture, with the perchlorate, was then lightly re-ground prior to SHS initiation.

Results

Sample preparation

Self-propagating high-temperature synthesis reactions were performed using various starting mixtures of Y_2O_3, Fe_2O_3, Fe, Cr_2O_3 and $NaClO_4$. The molar ratio of each reagent was chosen to conform with the desired stoichiometry in the product, Table 1. The reaction is driven by the exothermic oxidation of Fe metal by oxygen, which was evolved from the sodium perchlorate decomposition. The perchlorate fully decomposed to oxygen and salt (NaCl) at 600 °C. In the case of $Y_3Fe_{4.8}Cr_{0.2}O_{12}$ the reaction scheme is shown in eqn. (1)

$$3Y_2O_3 + 1.3Fe_2O_3 + 0.2Cr_2O_3 + 7Fe + 2.625NaClO_4 \rightarrow 2Y_3Fe_{4.8}Cr_{0.2}O_{12} + 2.625NaCl \quad (1)$$

It should be noted that all the reactions were carried out in air using only solid oxidisers. The co-produced sodium chloride melts during the reaction and acts as an internal wetting agent allowing inter-diffusion of the reactants. Notably it is readily removed after the reaction by trituration of the product with water. The SHS preparation of pure and chromium-substituted yttrium iron garnet is much quicker than standard conventional methods. Using SHS instead of the first annealing stage in the conventional synthesis reduces the reaction time from 24 h to *ca.* 10 s.

Two series of samples were prepared: series 1 by SHS followed by annealing at 1450 °C for 4 h, and series 2 by SHS in

Table 1 Millimoles of reagent used in self-propagating high-temperature synthesis of $Y_3Fe_{5-x}Cr_xO_{12}$, nominal composition of the end product, using a standard notation where parentheses denote tetrahedral sites and square brackets denote octahedral sites, and observed composition of selected samples as determined by electron probe or EDAX measurements

	mmol						
x	Fe	Fe_2O_3	Y_2O_3	Cr_2O_3	$NaClO_4$	Nominal composition	Observed composition
0	11.6	2.50	5.0	0	4.275	$Y_3[Fe_2](Fe_3)O_{12}$	$Y_{3.0}Fe_{5.0}O_{12}$
0.1	11.6	2.335	5.0	0.1	4.275	$Y_3[Fe_{1.9}Cr_{0.1}](Fe_3)O_{12}$	—
0.2	11.6	2.165	5.0	0.2	4.275	$Y_3[Fe_{1.8}Cr_{0.2}](Fe_3)O_{12}$	$Y_{3.0}Fe_{4.81}Cr_{0.21}O_{12}$
0.3	11.6	2.00	5.0	0.3	4.275	$Y_3[Fe_{1.7}Cr_{0.3}](Fe_3)O_{12}$	—
0.4	11.6	1.835	5.0	0.4	4.275	$Y_3[Fe_{1.6}Cr_{0.4}](Fe_3)O_{12}$	$Y_{2.94}Fe_{4.58}Cr_{0.42}O_{12}$[a]
0.5	11.6	1.665	5.0	0.5	4.275	$Y_3[Fe_{1.5}Cr_{0.5}](Fe_3)O_{12}$	$Y_{3.0}Fe_{4.51}Cr_{0.49}O_{12}$
0.6	11.6	1.50	5.0	0.6	4.275	$Y_3[Fe_{1.4}Cr_{0.6}](Fe_3)O_{12}$	$Y_{3.0}Fe_{4.41}Cr_{0.61}O_{12}$[a]

[a]Determined by EDAX measurement.

a magnetic field of 1.1 T, followed by annealing at 1450 °C for 4 h.

Characterisation

Electron microprobe mapping using a 1 μm spot size over a 10×10 μm grid (100 spots 10 μm apart) showed for $x=0$ a composition of $Y_{3.0}Fe_{5.0}O_{12.0}$ with $<2\%$ elemental variation between spots (see Table 1). For the applied field $x=0.5$ sample the average composition map revealed a composition of $Y_3Fe_{4.51}Cr_{0.49}O_{12}$ with minimal (*ca.* 1–2%) variation between spots. However, the zero field $x=0.6$ sample showed some inhomogeneity at a level of 4–5% corresponding to the formation of an $YCrO_3$ impurity phase. SEM and EDAX spot analysis agreed with these findings and showed that for low chromium concentrations a solid solution was formed, while at high chromium levels some degree of phase segregation occurred (for the $x=0.5$ and 0.6 samples). Notably, those samples prepared in an external field were more homogeneous than those prepared in zero field. SEM showed that the samples were composed of agglomerates of crystallites.

X-Ray powder diffraction showed a predominantly single-phase cubic structure for all the sintered products, with lattice parameters as given in Table 2. A general decrease in the *a* parameter with increasing chromium content was noted. This is in agreement with conventionally prepared materials.[22,23]

The FTIR spectra of the sintered pure and chromium substituted yttrium iron garnet samples showed three intense absorption bands in the range 4000–400 cm^{-1} at 656, 605 and 565 cm^{-1}. No identifiable starting materials were seen in the spectra and no quantifiable changes in absorption intensity could be matched with levels of chromium substitution. These three main absorptions can be attributed to metal oxygen lattice vibrations.

^{57}Fe Mössbauer absorption spectra were recorded for series 1 and 2 samples at room temperature (Fig. 1). The spectra were least squares fitted using Lorentzian lineshapes and combinations of quadrupole split doublets and magnetically split sextets. For all of the SHS samples two subcomponent sextets, attributed to octahedral and tetrahedral positions of the iron atoms, were fitted. Minority components in the form of an additional sextet and/or a centrally placed doublet or pair of doublets were also fitted as necessary. Representative spectra as fitted are shown as solid lines in Fig. 1, and parameters for all the samples obtained from these fits are given in Table 3.

Hysteresis loops were recorded on all the samples in fields up to 7.5 kOe. The maximum magnetisations σ_{max}, remanent magnetisations σ_r and coercive forces H_c thus obtained are listed in Table 4. Samples prepared in an external magnetic field (series 2) showed somewhat different magnetic parameters to those prepared in zero field. A general trend was noted, in that the series 2 samples exhibited larger σ_{max} and σ_r values and smaller H_c values than the corresponding series 1 samples for a given Cr content.

Table 2 Cubic lattice parameter *a* for two series of $Y_3Fe_{5-x}Cr_xO_{12}$ samples produced by self-propagating high-temperature synthesis (SHS): series 1; zero field SHS followed by annealing at 1450 °C for 4 h; series 2; SHS conducted in a magnetic field of 1.1 T followed by annealing at 1450 °C for 4 h

x	Series 1, a^a/Å	Series 2, a^a/Å
0	12.374	12.365
0.1	12.366	12.363
0.2	12.362	12.353
0.3	12.359	12.345
0.4	12.347	12.343
0.5	12.343	12.341
0.6	12.328	12.338

$^a \pm 0.004$ Å.

Discussion

Synthesis

SHS synthesis provides, after an annealing stage, a relatively straightforward method of producing stoichiometric $Y_3Fe_5O_{12}$. When conducted in an applied magnetic field the reaction produced a more homogeneous product than did the corresponding zero field synthesis. This is probably a consequence of a hotter synthesis wave. The magnetic starting components Fe and Fe_2O_3 are partially aligned by the magnetic field, and this allows a more complete reaction to proceed. Sintering of the applied field SHS product is more facile and produces larger particles than is possible from the zero field SHS product. The resultant differences in microstructure may explain the observed differences in the magnetic properties of the samples prepared *via* zero field and applied field reactions.

X-Ray measurements

The variation in unit cell size may be attributed to the smaller ionic radii of six-fold co-ordinated Cr^{3+} (0.64 Å) compared to that of six-fold high spin Fe^{3+} (0.67 Å).[24] It has been previously established that the location of substituted ions within yttrium ferrite garnet is largely dependent on ionic size. In yttrium iron garnet the tetrahedral sites are much smaller than the octahedral sites, and ions with smaller ionic radii than iron tend to congregate in the tetrahedral sites. Despite this, chromium preferentially replaces iron from the octahedral sites within the garnets because of favourable crystal field effects.

Some traces of a $YCrO_3$ impurity phase were seen for the highest Cr content zero field sample (*ca.* 10% $YCrO_3$ for $x=0.6$), which is not unexpected given the high Cr content of this sample. However, the other zero field samples, and all the applied field samples, were on inspection found to be almost entirely monophasic. It is interesting to note that this is somewhat at odds with the observation by Villers *et al.*[14] of a second, orthorhombic phase (*i.e.* $YCrO_3$) in samples with $x \geqslant 0.4$ made by conventional ceramic means. We infer that either the SHS route provides a superior means of obtaining monophase products, or that if there are $YCrO_3$ impurities in the SHS samples, they must occur in a fine particle form which escapes detection by standard X-ray diffraction measurements.

Another notable difference between the SHS prepared garnets and ceramic route samples is that the measured cubic lattice parameters are somewhat smaller. For example, reported lattice parameters of 12.376 Å[16] and 12.377 Å[25] for conventionally prepared $Y_3Fe_5O_{12}$, and of 12.368 Å[16] for $Y_3Fe_{4.75}Cr_{0.25}O_{12}$, are all larger than found in the corresponding SHS samples. Similar differences in lattice parameter have been noted in a range of ceramics formed by SHS reactions,[26,27] with the effect (albeit not fully understood) being associated with the very high reaction temperatures and fast cooling rates of the combustion wave. In this context it is furthermore interesting to note that the lattice parameters measured in the series 2 samples are consistently less than in the series 1 samples, which again may be correlated with the hotter reaction conditions occurring in the presence of an applied magnetic field. Conclusive evidence of similar effects have recently been reported in zero field *versus* applied field SHS preparations of the M-type ferrite $BaFe_{12}O_{19}$.[28]

Mössbauer measurements

Room temperature Mössbauer spectra for the SHS prepared $Y_3Fe_{5-x}Cr_xO_{12}$ show two well resolved sextets from the iron atoms in the octahedral (*a*) and tetrahedral (*d*) sublattices (Fig. 2). The relative spectral areas of these sextets were found to be satisfactorily fitted under the hypothesis that they were in the ratio $(2-x):3$, as would be the case if only the octahedral Fe sites were substituted with Cr. Note that this assumes that

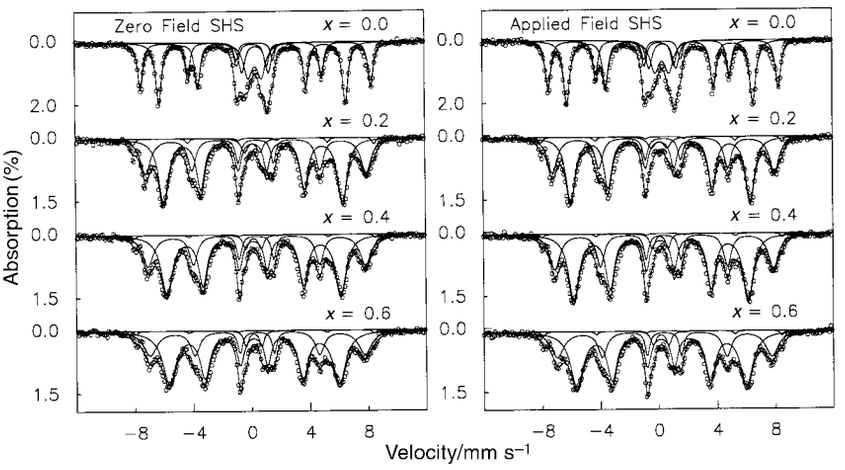

Fig. 1 Representative room temperature Mössbauer spectra for $Y_3Fe_{5-x}Cr_xO_{12}$ ferrite-garnets prepared by SHS reactions in zero field or in an external field of 1.1 T, subsequently annealed at 1450 °C for 4 h. The solid lines show the results of least-squares fits to the data, as discussed in the text and in Table 3.

the recoil free fractions for both octahedral and tetrahedral Fe are the same; the generally good quality of the fits seems to validate this assumption.

The difference in hyperfine fields between the sublattices is due to the different degrees of covalency for the Fe^{3+} ions in the *a* and *d* sites of the garnet crystal lattice. The hyperfine fields were larger for the octahedral site than for the tetrahedral site: 49.0 T compared to 39.6 T for the pure yttrium iron garnet sample. These values of hyperfine field are comparable to those found in conventionally prepared materials.[29] Increasing the amount of Cr substitution reduces the hyperfine fields of both the *a* and *d* sites (see Fig. 2). The reduction in the hyperfine field of the tetrahedral sublattice is due to the reduction of the strong exchange interactions between the *a* and *d* sites. The measured reduction in hyperfine field varies linearly with Cr content (see Fig. 2), implying that the degree of Cr substitution on the octahedral site is closely correlated to the Cr content in the SHS product.

The sublattice linewidths increased with Cr substitution (see Table 3), as expected given the disruption in local environment around the Fe atoms. The best model for fitting these linewidths was found to be one in which the outer, middle and inner pairs of lines in each sublattice sextet were assigned linewidths $\Gamma+\Delta\Gamma$, Γ and $\Gamma-\Delta\Gamma$ respectively, where $\Delta\Gamma$ is a measure of the spread in hyperfine fields at the Fe atoms. To aid interpretation of these data, a weighted mean linewidth $\bar{\Gamma}=\frac{1}{6}[(2-x)\bar{\Gamma}_{oct}+3\bar{\Gamma}_{tet}$ was calculated, where $\bar{\Gamma}_{oct}$ and $\bar{\Gamma}_{tet}$ were the mean sublattice linewidths estimated by taking into account the 3 : 2 : 1 area ratios of the outer : middle : inner pairs of lines, $\bar{\Gamma}_{oct/tet}=\Gamma+\frac{1}{3}\Delta\Gamma$. The variations in $\bar{\Gamma}$ for the series 1 and 2 samples, as a function of Cr content, are shown in Fig. 2. They are essentially linear, consistent with progressive lattice disruption as the Cr occupies the octahedral sites.

In addition to the well resolved octahedral and tetrahedral sublattice $Y_3Fe_{5-x}Cr_xO_{12}$ sextets discussed above, in most samples an additional paramagnetic doublet contribution was seen. This was particularly so at the lower levels of chromium substitution. Although the origin of this contribution has not been rigorously tested, the fact that no additional phases were apparent in the X-ray data leads us to surmise that it is due to some superparamagnetic $Y_3Fe_{5-x}Cr_xO_{12}$ crystallites in the product. For higher Cr contents a very small (1–2% of the total spectral area) minority phase is apparent, in the form of a magnetic sextet with a large hyperfine field of the order 51.0 T. This sextet is identifiable as due to an iron oxide, most probably hematite, α-Fe_2O_3. It is not surprising that such a

Table 3 Room temperature Mössbauer data for $Y_3Fe_{5-x}Cr_xO_{12}$ ferrite-garnets prepared by SHS reactions in zero field or in an external field of 1.1 T (series 1 and 2), subsequently annealed at 1450 °C for 4 h. The parameters listed are the isomer shift δ ($\pm$0.01 mm s^{-1}), quadrupole shift 2ε ($\pm$0.02 mm s^{-1}), linewidths Γ and $\Delta\Gamma$ ($\pm$0.02 mm s^{-1}), and hyperfine field B_{hf} ($\pm$0.3 T) of the octahedral and tetrahedral sites in the ferrite-garnet structure. The relative areas of these sextets were constrained to the ratio $(2-x):3$, in accordance with a model in which all the Cr ions reside on the octahedral sites. Also listed are the relative spectral areas of two additional phases identified in the spectra: a paramagnetic doublet component (PM) due to superparamagnetic fine particles of $Y_3Fe_{5-x}Cr_xO_{12}$, and a magnetic sextet (Ox) due to an iron oxide impurity

	Octahedral sites					Tetrahedral sites						
x	δ	2ε	Γ	$\Delta\Gamma$	B_{hf}	δ	2ε	Γ	$\Delta\Gamma$	B_{hf}	%PM	%Ox
Zero field SHS												
0	0.37	0.07	0.37	0.04	49.0	0.14	0.03	0.42	0.03	39.6	29	—
0.1	0.37	0.07	0.42	0.07	48.5	0.15	0.02	0.48	0.09	39.1	29	—
0.2	0.37	0.00	0.63	0.23	46.9	0.15	0.03	0.67	0.12	38.0	4	2
0.3	0.37	0.04	0.46	0.09	47.8	0.15	0.02	0.58	0.11	38.2	10	4
0.4	0.37	0.02	0.65	0.26	46.2	0.15	0.03	0.73	0.20	36.9	4	1
0.5	0.39	0.01	0.71	0.29	46.0	0.15	0.01	0.79	0.22	36.4	3	1
0.6	0.38	0.02	0.74	0.34	45.7	0.15	0.01	0.84	0.25	36.1	3	1
Applied field SHS												
0	0.38	0.06	0.39	0.04	48.8	0.15	0.03	0.45	0.04	39.4	26	—
0.1	0.37	0.07	0.48	0.14	48.5	0.15	0.01	0.51	0.19	38.8	53	—
0.2	0.37	0.01	0.62	0.20	47.1	0.15	0.02	0.64	0.11	38.1	4	2
0.3	0.38	−0.02	0.68	0.27	46.6	0.14	0.03	0.73	0.16	37.3	4	1
0.4	0.38	0.02	0.62	0.23	46.4	0.15	0.02	0.70	0.17	37.0	3	1
0.5	0.38	0.00	0.67	0.28	46.1	0.15	0.02	0.79	0.21	36.5	2	1
0.6	0.38	0.01	0.70	0.34	45.6	0.16	0.02	0.81	0.24	36.0	3	2

Table 4 Room temperature magnetic properties of $Y_3Fe_{5-x}Cr_xO_{12}$ ferrite-garnets prepared by zero field SHS and SHS in a magnetic field of 1.1 T: maximum magnetisation σ_{max} in an external field of 7.5 kOe (± 0.2 emu g^{-1}); remanent magnetisation σ_r (± 0.1 emu g^{-1}) and coercive force H_c (± 0.2 Oe)

	Zero field SHS			SHS in field of 1.1 T		
x	σ_{max}	σ_r	H_c	σ_{max}	σ_r	H_c
0	14.60	1.03	4.9	15.80	1.39	4.2
0.1	15.36	1.29	4.5	16.28	1.54	4.0
0.2	16.27	1.51	4.2	17.22	1.70	3.6
0.3	20.34	2.12	4.0	21.14	2.39	3.1
0.4	18.90	1.88	5.1	19.75	2.01	4.4
0.5	18.40	1.74	5.7	18.77	1.80	4.6
0.6	17.21	1.66	7.0	18.04	1.75	6.0

small contribution was not apparent in the X-ray data, especially since it may well exist in a fine particle form.

Magnetic measurements

The magnetic data in Fig. 3 illustrate that the same underlying trends appear in both the series 1 and 2 sets of samples, and that the applied field samples show consistently higher magnetisations and lower coercivities. The most likely cause for this is improved crystallinity in the applied field samples.

Yttrium iron garnet is characterised by strong antiferromagnetic interactions between the Fe^{3+} ions on the *a* and *d* sublattices. As the Y^{3+} ions are non-magnetic, theoretically the calculated magnetic moment σ_0 (μ_B) per formula unit $Y_3Fe_5O_{12}$ is $\sigma_0 = 3\sigma_d - 2\sigma_a$, where σ_d and σ_a are the magnetic moments of the Fe^{3+} ions in the *d* and *a* sublattices ($\mu_{Fe^{3+}} = 5\ \mu_B$).[5,10,13] For pure yttrium iron garnet the magnetic moment value is 5 μ_B per formula unit. For chromium substitution, taking into account the preference for octahedral coordination results in a magnetic moment per formula unit given by:

$$\sigma_0 = \{3\sigma_d - [(2-x)\sigma_a + x\sigma'_a]\} \quad (2)$$

where σ'_a is the magnetic moment of Cr^{3+} ion ($\mu_{Cr^{3+}} = 3\mu_B$) and

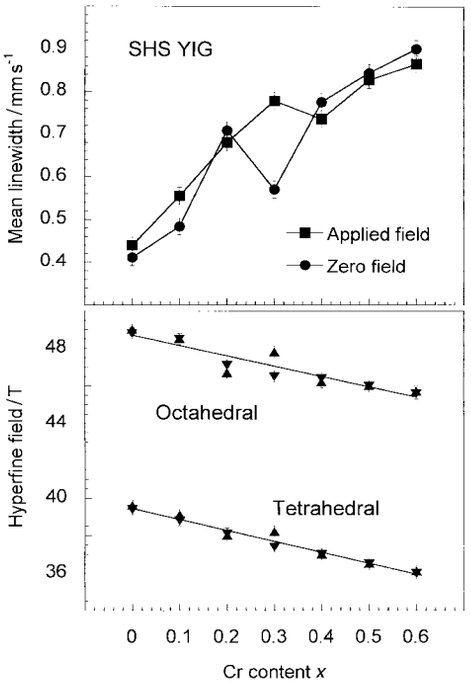

Fig. 2 Variation with Cr content *x* of (i) the magnetic hyperfine fields of the octahedral and tetrahedral sites and (ii) the weighted mean linewidths (as discussed in the text) deduced from the Mössbauer spectra of $Y_3Fe_{5-x}Cr_xO_{12}$ samples prepared by SHS reactions in zero field (▲) or in an applied field of 1.1 T (▼), subsequently annealed at 1450 °C for 4 h.

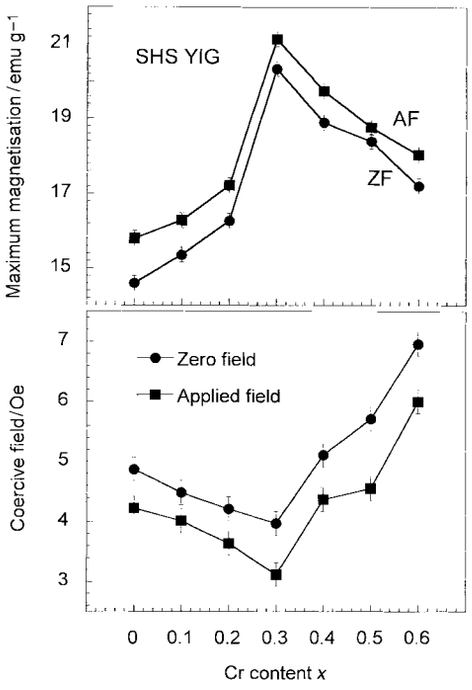

Fig. 3 Variation with Cr content *x* of (i) the bulk magnetisation and (ii) the coercive force, measured in an applied field of 7.5 kOe, for $Y_3Fe_{5-x}Cr_xO_{12}$ samples prepared by SHS reactions in zero field or in an applied field of 1.1 T, subsequently annealed at 1450 °C for 4 h.

x is the degree of substitution. From this formula the resultant magnetic moment should increase linearly with *x* (at $x = 0.1$, $\sigma_0 = 5.2\ \mu_B$ and at $x = 0.6$ $\sigma_0 = 6.2\ \mu_B$).[10]

The variation in maximum measured magnetisation σ_{max} with Cr content in the SHS prepared materials, shown in Fig. 3, does not comply with this model. Although the $x = 0$, 0.1 and 0.2 samples show a linear increase in σ_{max} with a slope in accordance with expectation, a sharp peak is seen in both the zero field and applied field SHS samples for $x = 0.3$. At higher Cr contents the magnetisation then falls steadily with increasing Cr. Also shown in Fig. 3 is the H_c data, which also indicate a change in magnetic behaviour at $x = 0.3$, where a minimum is reached. For $x = 0.4$ and above a sharp increase in H_c is seen.

The shape of the magnetisation *vs.* Cr content curve in Fig. 3 is similar to that observed by Villers *et al.*[14] for the low temperature extrapolated specific magnetisation in conventionally prepared $Y_3Fe_{5-x}Cr_xO_{12}$. Villers *et al.* attributed the fall in magnetisation for $x \geqslant 0.4$ to the formation of an antiferromagnetic $YCrO_3$ impurity phase at the expense of the cubic yttrium iron garnet phase. Even though our X-ray evidence showed no new phases at or near $x = 0.4$ in the SHS samples, the Mössbauer results indicate some iron oxide impurities (at a level of 1–2%) in all the samples with $x \geqslant 0.2$. To

preserve the elemental composition of the samples we expect that the two impurity phases should co-exist. Thus it is likely that both $YCrO_3$ and α-Fe_2O_3 are present in the higher Cr-content samples. Thus a possible explanation for the fall in magnetisation with increasing Cr content is the increased presence of non-magnetic impurities.

There is however a peculiarity in the coercivity data. The observed steady increase in H_c for $x \geqslant 0.3$ may at first sight also be attributed to the presence of impurity phases. However, given that we expect that the contribution of antiferromagnetic $YCrO_3$ to the hysteresis data will be negligible, the observed coercivity increase must be associated with the presence of the weakly ferromagnetic (canted antiferromagnet) α-Fe_2O_3 phase. This leaves open the question as to how or why the coercivity of the α-Fe_2O_3 phase should be increasing in a nearly monotonic fashion as the Cr content of the samples increases. More detailed investigation would probably be needed to address this matter, which is perhaps a microstructural effect.

Nevertheless, we note in passing an alternative explanation for the observed fall in magnetisation and rise in coercivity, which does not rely on impurity phases, but rather is based on magnetic frustration and percolation. According to theory,[30] the critical percolation concentration for sites occupying a simple cubic lattice is 0.311. At this concentration all the dopant atoms on the lattice 'see' each other as a single infinite cluster. If the dopant atoms are antiferromagnetically coupled Cr^{3+} ions and the host atoms are ferromagnetically coupled Fe^{3+} ions, then at the percolation concentration the Cr^{3+} ions could impose a frustrated magnetic configuration on the system. This would be apparent as both a fall in the obtainable magnetisation and an increased coercivity, as it becomes more difficult to manipulate the system with an external field. Although not directly applicable to the $Y_3Fe_{5-x}Cr_xO_{12}$ system (because Cr^{3+} preferentially occupies the octahedral Fe^{3+} sites, and because the interactions are an oxygen mediated superexchange), the model as described does indicate that such effects could be present and could give rise to the observed data.

Conclusions

Representative chromium-substituted yttrium iron garnet magnets, $Y_3Fe_{5-x}Cr_xO_{12}$, have been prepared for the first time by a process involving initial reaction *via* self-propagating high-temperature synthesis (SHS) followed by annealing at 1450 °C for 4 h. The reactions are straightforward and easy to perform, and yield nearly phase pure products in much shorter synthesis times, and with much less input of external energy, than in conventional syntheses. Mössbauer effect experiments established that Cr substitution was successfully accomplished, with the Cr^{3+} ions supplanting Fe^{3+} ions on the octahedral sublattice of the garnet structure. Samples prepared by SHS reaction in an applied magnetic field, followed by annealing, showed significantly larger specific magnetisations and smaller coercivities than were found in equivalent samples produced by zero field SHS, followed by annealing. These results are consistent with changes in the microstructure of the products, influenced by the applied magnetic field during the SHS reaction, such as a tendency to form larger sized crystallites in the applied field reactions. In both sets of samples a magnetisation maximum and coercivity minimum was seen at $x = 0.3$, possibly due to the presence of increasing amounts of $YCrO_3$ and α-Fe_2O_3 impurities in the higher Cr content samples.

Acknowledgements

M.V.K. thanks both the Royal Society and the Royal Society of Chemistry Journal Fund for short-term visitors grants which have facilitated this work. The Mössbauer spectra were collected under the auspices of the University of London Intercollegiate Research Service.

References

1 F. Bertaut and F. Forrat, *Compt. Rend. Acad. Sci. Paris*, 1956, **242**, 382.
2 S. Geller and M. A. Gilleo, *Acta Crystallogr.*, 1957, **10**, 239.
3 Y. Yamazaki, T. Namimawa, T. Hirano and K. Yoshida, *J. Phys. IV*, 1997, **7**, C1.
4 R. Pauthenet, *Compt. Rend. Acad. Sci. Paris*, 1956, **243**, 1499.
5 R. Pauthenet, *Ann. Phys.*, 1958, **3**, 428.
6 L. Néel, *Compt. Rend. Acad. Sci. Paris*, 1954, **239**, 8.
7 R. Aleonard, M. Barbier and R. Pauthenet, *Compt. Rend. Acad. Sci. Paris*, 1956, **242**, 2531.
8 Y. J. Song, G. B. Turpin, R. E. Bornfreund, H. Aoyama and P. E. Wigan, *J. Magn. Mater.*, 1996, **154**, 37.
9 A. A. Gusev and A. S. Pahomov, *Izv. AN SSSR Ser. Fiz.*, 1961, **25**, 1327.
10 K. P. Belov and M. A. Zaitseva, in *Ferrites: physical properties of ferromagnetic oxides in relation to their technical applications*, ed. J. Smit and H. P. Wijn, Philips Technical Library, Eindhoven, Netherlands, 1959, p. 457.
11 M. A. Gilleo, *Phys. Rev.*, 1958, **109**, 777.
12 G. Villers and J. Loriers, *Compt. Rend. Acad. Sci. Paris*, 1957, **245**, 2033.
13 M. A. Gilleo and S. Geller, *Phys. Rev.*, 1958, **110**, 73.
14 G. Villers, R. Pauthenet and J. Loriers, *J. Phys. Radium*, 1958, **20**, 382.
15 R. Pauthenet, *J. Appl. Phys.*, 1958, **29**, 253.
16 M. A. Gilleo and S. J. Geller, *J. Appl. Phys.*, 1958, **29**, 380.
17 G. A. Sawatzky, F. van der Woude and A. H. Morrish, *Phys. Rev.*, 1969, **183**, 383.
18 I. S. Lyubutin, in *Physics and chemistry of ferrites*, ed. I. S. Belov and Y. D. Tretyakov, Moscow University, Moscow, 1973, p. 68.
19 Q. A. Pankhurst and I. P. Parkin, *Mater. World*, 1998, 743.
20 I. P. Parkin, M. V. Kuznetsov and Q. A. Pankhurst, *J. Mater. Chem.*, 1999, **9**, 273.
21 W. B. Cross, L. Affleck, M. V. Kuznetsov, I. P. Parkin and Q. A. Pankhurst, *J. Mater. Chem.*, 1999, **9**, 2545.
22 E. W. Gorter, *Philips Res. Rep.*, 1954, **9**, 295.
23 F. C. Romeijn, *Philips Res. Rep.*, 1953, **8**, 304.
24 R. Shanon and C. T. Prewitt, *Acta Crystallogr., Sect. B*, 1969, **25**, 925.
25 V. D. Murumkar, K. B. Modi, K. M. Jadhav, G. K. Bichile and R. G. Kulkarni, *Mater. Lett.*, 1997, **32**, 281.
26 A. G. Merzhanov, *J. Mater. Process. Technol.*, 1996, **56**, 222.
27 V. Auselmi-Tamburini, M. Armondi, F. Maglia, G. Spinola and Z. A. Munir, *J. Am. Ceram. Soc.*, 1998, **81**, 1705.
28 M. D. Aguas, L. Affleck, I. P. Parkin, M. V. Kuznetsov, W. A. Steer, Q. A. Pankhurst, L. Fernández Barquín, M. A. Roberts, M. I. Boamfa and J. A. A. J. Perenboom, *J. Mater. Chem.*, 2000, **10**, 235.
29 P. C. Dorsey, S. E. Bushnell, R. G. Seed and C. Vittoria, *IEEE Trans. Mag.*, 1993, **29**, 3069.
30 See, for example: S. R. Elliott, *Physics of amorphous materials*, Longman Scientific & Technical, London, 2nd edn., 1990, p. 299.

Paper a909007j